Acta Crystallographica Section F
Structural Biology and Crystallization Communications
ISSN 1744-3091

Structures of hypoxanthine-guanine phosphoribosyltransferase (TTHA0220) from *Thermus thermophilus* HB8

Mayumi Kanagawa,[a] Seiki Baba,[a] Akio Ebihara,[a]‡ Akeo Shinkai,[a] Ken Hirotsu,[a] Ryosuke Mega,[b] Kwang Kim,[b] Seiki Kuramitsu,[a,b] Gen-ichi Sampei[a,c] and Gota Kawai[a,d]*

[a]RIKEN SPring-8 Center, Harima Institute, 1-1-1 Kouto, Sayo, Hyogo 679-5148, Japan, [b]Department of Biological Sciences, Graduate School of Science, Osaka University, Toyonaka, Osaka 560-0043, Japan, [c]Department of Applied Physics and Chemistry, University of Electro-Communications, 1-5-1 Chofugaoka, Chofu, Tokyo 182-8585, Japan, and [d]Department of Life and Environmental Sciences, Faculty of Engineering, Chiba Institute of Technology, Narashino, Chiba 275-0016, Japan

‡ Present address: Faculty of Applied Biological Sciences, Gifu University, 1-1 Yanagido, Gifu 501-1193, Japan.

Correspondence e-mail: gkawai@sea.it-chiba.ac.jp

Received 26 April 2010
Accepted 15 June 2010

PDB References: hypoxanthine-guanine phosphoribosyltransferase, 3acb; GMP complex, 3acc; IMP complex, 3acd.

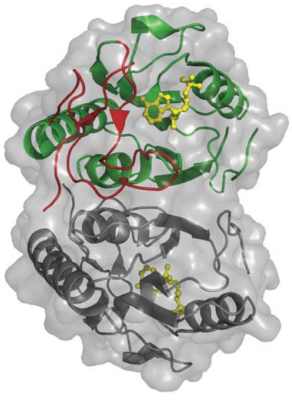

Hypoxanthine-guanine phosphoribosyltransferase (HGPRTase), which is a key enzyme in the purine-salvage pathway, catalyzes the synthesis of IMP or GMP from α-D-phosphoribosyl-1-pyrophosphate and hypoxanthine or guanine, respectively. Structures of HGPRTase from *Thermus thermophilus* HB8 in the unliganded form, in complex with IMP and in complex with GMP have been determined at 2.1, 1.9 and 2.2 Å resolution, respectively. The overall fold of the IMP complex was similar to that of the unliganded form, but the main-chain and side-chain atoms of the active site moved to accommodate IMP. The overall folds of the IMP and GMP complexes were almost identical to each other. Structural comparison of the *T. thermophilus* HB8 enzyme with 6-oxopurine PRTases for which structures have been determined showed that these enzymes can be tentatively divided into groups I and II and that the *T. thermophilus* HB8 enzyme belongs to group I. The group II enzymes are characterized by an N-terminal extension with additional secondary elements and a long loop connecting the second α-helix and β-strand compared with the group I enzymes.

1. Introduction

Purine nucleotides are of central importance to the biosynthesis of DNA, RNA and several cofactors such as ATP and FAD. There are two interrelated pathways for the synthesis of purine nucleotides: the *de novo* and salvage pathways. Hypoxanthine-guanine phosphoribosyltransferase (HGPRTase) is a key enzyme in the purine-salvage pathway and reversibly catalyzes the transfer of the 5-phophoribosyl group from α-D-phosphoribosyl-1-pyrophosphate (PRPP) to hypoxanthine or guanine to form inosine 5′-monophosphate (IMP) or guanosine 5′-monophosphate (GMP), respectively (Fig. 1). HGPRTase deficiency is responsible for Lesch–Nyhan syndrome in humans (Lesch & Nyhan, 1964). Most protozoan parasites are deficient in the *de novo* purine-biosynthesis pathway. Therefore, HGPRTase involved in the salvage pathway is a potential target for the development of antiparasitic agents (Wang, 1984; Ullman & Carter, 1995).

To date, the structures of 6-oxopurine PRTases from *Homo sapiens* (Eads *et al.*, 1994; Shi, Li, Tyler, Furneaux, Grubmeyer *et al.*, 1999; Keough *et al.*, 2005), *Toxoplasma gondii* (Schumacher *et al.*, 1996; Héroux *et al.*, 2000), *Tritrichomonas foetus* (Somoza *et al.*, 1996), *Trypanosoma cruzi* (Focia, Craig & Eakin, 1998; Canyuk *et al.*, 2001), *Plasmodium falciparum* (Shi, Li, Tyler, Furneaux, Cahill *et al.*, 1999), *Escherichia coli* (Guddat *et al.*, 2002), *Thermoanaerobacter tengcongensis* (Chen *et al.*, 2005) and *Leishmania tarentolae* (Monzani *et al.*, 2007) have been reported in order to elucidate the structure–function relationship of 6-oxopurine PRTases. These structures show a common α/β fold and four flexible loops (loops I–IV). The loops are highly mobile and change their conformations depending on the binding of inhibitors, substrates or products. To elucidate the overall and the active-site structure and the enzyme–IMP or enzyme–GMP interactions, we determined the crystal structures of HGPRTase from *Thermus thermophilus* HB8 (*Tt*HGPRTase) in the unliganded form, of *Tt*HGPRTase complexed with IMP and of *Tt*HGPRTase complexed with GMP. Structural comparison of *Tt*HGPRTase with

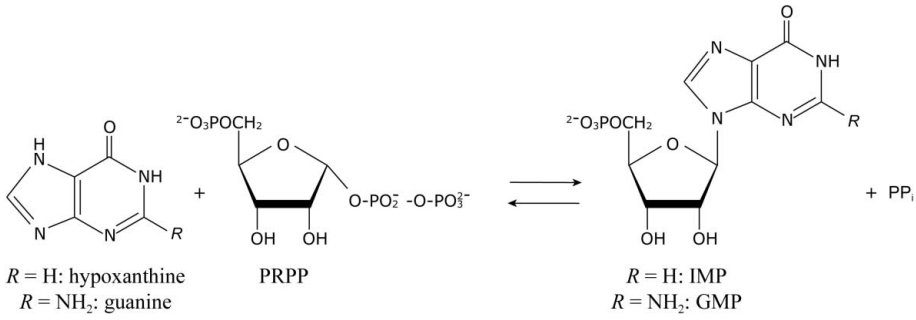

Figure 1
The reaction catalyzed by HGPRTase.

the related 6-oxopurine PRTases provided some insight into the classification of these enzymes.

2. Materials and methods

2.1. Reagents

Guanine, hypoxanthine, xanthine, GMP, IMP, XMP, 5′-phosphoribosyl-1′-pyrophosphate (PRPP), dibutylamine and formic acid were obtained from Sigma–Aldrich Inc. (St Louis, USA). Acetonitrile (LC/MS grade) was purchased from Wako Co. (Osaka, Japan). All reagents were of the highest grade commercially available.

2.2. Protein expression and purification

The TTHA0220 gene was amplified by PCR using *T. thermophilus* HB8 genomic DNA as the template. The amplified fragment was cloned under the control of the T7 promoter of the *E. coli* expression vector pET-11a (Novagen, Madison, Wisconsin, USA). The expression vector was introduced into *E. coli* BL21 (DE3) strain (Novagen) and the recombinant strain was cultured in 6 l LB medium supplemented with 50 mg ml^{-1} ampicillin. The collected cells (19.0 g) were suspended in 20 m*M* Tris–HCl buffer pH 8.0 containing 50 m*M* NaCl and disrupted by sonication. The cell lysate was incubated at 343 K for 10 min and kept on ice for 12 min. After ultracentrifugation at 200 000*g* and 277 K, the soluble fraction was applied onto a Resource ISO column (GE Healthcare, UK) equilibrated with 50 m*M* sodium phosphate buffer pH 7.0 containing 1.5 *M* ammonium sulfate and was eluted with a linear gradient of 1.5–0 *M* ammonium sulfate. *Tt*HGPRTase fractions were applied onto a Resource Q column (Amersham Biosciences) equilibrated with 20 m*M* Tris–HCl pH 8.0, which was eluted with a linear gradient of 0–0.5 *M* NaCl. The fractions containing *Tt*HGPRTase were applied onto a hydroxyapatite CHT10-I (Bio-Rad) column equilibrated with 0.01 *M* sodium phosphate buffer pH 7.0 containing 150 m*M* NaCl and eluted with a linear gradient of 0.01–0.5 *M* sodium phosphate buffer containing 150 m*M* NaCl. The collected *Tt*HGPRTase fractions were applied onto a HiLoad 16/60 Superdex 75 column (GE Healthcare, UK) equilibrated with 20 m*M* Tris–HCl pH 8.0 containing 150 m*M* NaCl. The protein solution was desalted on a HiPrep 26/10 desalting column (GE Healthcare, UK) and concentrated to 10.3 mg ml^{-1}. The protein concentration was estimated from the UV absorption at 260 nm. The overall yield was estimated to be 19 mg from 6 l of culture.

2.3. Enzyme assays

The enzyme activity was measured at various concentrations of guanine, hypoxanthine or xanthine in the presence of 2 n*M* enzyme, 1 m*M* PRPP, 50 m*M* Tris–HCl, 100 m*M* KCl and 10 m*M* $MgCl_2$ at pH 7.8 and 298 K. The reaction products were analyzed by ion-pair reverse-phase chromatography using a CAPCELL PAK C18 column (Shiseido Fine Chemicals, Tokyo, Japan) on an ÄKTA system (GE Healthcare, UK). The column was equilibrated with buffer containing 50 m*M* sodium phosphate pH 7.0, 5 m*M* tetra-*n*-butylammonium hydroxide and 0.25% methanol and eluted with a linear gradient of methanol from 0.25% to 30%. Products and reactants were quantified by measuring their absorbance at 256 and 276 nm. Kinetic constants were determined by fitting the Michaelis–Menten-type equation $k_{app} = k_{cat}[S]/([S] + K_M)$.

In order to confirm the reaction products, an APEX IV 9.4 T FT-ICR mass spectrometer with Apollo electrospray ionization (ESI) source (Bruker, USA) controlled by *apexControl* v.2.0.0 beta-version software for Windows XP was used. The mass spectrometer was operated in negative mode with 4500 and 4000 V voltages for the capillary and spray shield, respectively. The capillary exit was set to −90 V and the ion-accumulation time and flight time were set to 0.5 and 0.0018 s, respectively. All other parameters were optimized by a standard tuning procedure using ES Tuning Mix (Agilent Technologies, USA) under negative mode and calibrated by 1.0 p.p.m. error tolerance. An ÄKTA Explorer system (GE Healthcare, UK) was used to separate the reaction products and confirm each retention time with a flow rate of 25 µl min^{-1} using a CAPCELL PAK C18 column with a resin diameter of 3 µm, an inner diameter of 1.0 mm and a column length of 75 mm (Shiseido, Tokyo, Japan) and a binary gradient which consisted of the following HPLC-gradient solvents: *A*, 4 m*M* dibutylammonium formate (DBAF) pH 8.4; *B*, 4 m*M* DBAF pH 8.4, 50% acetonitrile. The gradient was as follows: 0–5 min, 5% *B* linear; 5–55 min, 60% *B* gradient; 55–60 min, 100% *B* gradient; 60–80 min, 100% *B* linear. 5 µl of each reaction mixture was injected manually using a 20 µl syringe (Hamilton, Switzerland) and the nucleoside monophosphate and PRPP standards were analyzed using the same gradient. The total ion chromatogram and the exact molecular weight of each result produced by FT-ICR/MS were further analyzed by *DataAnalysis* v.3.4 software (Bruker Daltonics, USA). The theoretical ion *m*/*z* of each product and the cofactor PRPP were calculated as follows: GMP, [*M*-H]$^-$, *m*/*z* 362.050723; XMP, [*M*-H]$^-$, *m*/*z* 364.042563; IMP, [*M*-H]$^-$, *m*/*z* 347.039823; PRPP, [*M*-H]$^-$, *m*/*z* 388.944538.

2.4. Crystallization, data collection and structure determination

The unliganded *Tt*HGPRTase was crystallized by the hanging-drop vapour-diffusion method. 1 µl protein solution (10.33 mg ml^{-1}) was mixed with an equal volume of a reservoir solution consisting of 38% dioxane, 15% glycerol and 18 m*M* Tris–HCl buffer pH 8.0 and equilibrated against 100 µl reservoir solution at 293 K. Crystals of *Tt*HGPRTase–IMP and TtHGPRTase–GMP were obtained under the same conditions as used for the unliganded enzyme, except for the concentration of dioxane (29 and 26%, respectively) and the presence of ligands (10 m*M* IMP and 5 m*M* GMP, respectively). All of the crystals are isomorphous, with space group $P6_522$ and unit-cell parameters $a = b = 66.7$, $c = 152.6$ Å for the apoenzyme, $a = b = 67.3$, $c = 152.2$ Å for the IMP complex and $a = b = 67.1$, $c = 152.5$ Å for the GMP complex. There is one monomer in the asymmetric unit and ∼49% of the crystal volume is occupied by solvent.

Table 1
Data-collection and refinement statistics.

Values in parentheses are for the highest resolution shell.

	Unliganded	IMP complex	GMP complex
PDB code	3acb	3acd	3acc
Space group	$P6_522$	$P6_522$	$P6_522$
Unit-cell parameters (Å)			
$a = b$	66.7	67.3	67.1
c	152.6	152.1	152.5
Diffraction data			
Resolution (Å)	2.06 (2.13–2.06)	1.89 (1.96–1.89)	2.16 (2.24–2.16)
Measured reflections	23534	30961	19318
No. of unique reflections	12932	17152	10794
Completeness (%)	99.8 (98.3)	99.9 (100.0)	93.2 (72.2)
$R_{\rm merge}$† (%)	8.8 (31.9)	4.5 (14.1)	8.6 (16.3)
$I/\sigma(I)$	36.1 (6.0)	67.4 (24.2)	32.5 (16.6)
Refinement			
Resolution limits (Å)	46.06–2.06	33.7–1.89	38.3–2.16
R factor (%)	20.1 (20.8)	19.9 (20.3)	21.0 (26.0)
$R_{\rm free}$ (%)	22.8 (26.3)	23.5 (26.8)	25.0 (32.6)
Test-set size for $R_{\rm free}$ (%)	10.3	10.3	10.3
No. of atoms			
Protein	1308	1295	1308
Ligands	12	35	36
Waters	127	185	107
Deviations from ideal geometry			
Bond lengths (Å)	0.005	0.006	0.006
Bond angles (°)	1.80	2.20	2.00
Mean B factors (Å^2)			
Main-chain atoms	24.98	19.19	22.83
Side-chain atoms	28.33	22.56	26.38
Ligand atoms	—	18.03	20.35
Water atoms	42.10	34.68	32.41
Ramachandran plot (%)			
Favoured	91.4	91.3	92.9
Additional allowed	7.9	8.0	6.4
Generously allowed	0.7	0.7	0.7
Disallowed	0.0	0.0	0.0

† $R_{\rm merge} = \sum_{hkl}\sum_i |I_i(hkl) - \langle I(hkl)\rangle| / \sum_{hkl}\sum_i I_i(hkl)$, where $I_i(hkl)$ is the observed intensity and $\langle I(hkl)\rangle$ is the average intensity for multiple measurements.

Diffraction data sets were collected at 100 K using a wavelength of 1.0000 Å on the RIKEN Structural Genomics Beamline II (BL26B2; Ueno *et al.*, 2006) at SPring-8 (Hyogo, Japan). All crystals were mounted on nylon loops and flash-cooled to 100 K in an N_2-gas stream. The crystals were then handled using the SPring-8 Precise Automatic Cryo-sample Exchanger (SPACE), which was controlled using the beamline-scheduling software *BSS* (Ueno *et al.*, 2004, 2005). All data were processed using the *HKL*-2000 program package (Otwinowski & Minor, 1997; Table 1).

The structure of *Tt*HGPRTase was solved by the molecular-replacement method using *AMoRe* (Navaza, 1994) with the *T. tengcongensis* structure (PDB code 1yfz; sequence identity 49%; Chen *et al.*, 2005) as a search model. The program *CNS* (Brünger *et al.*, 1998) was used for refinement cycles. After each round of refinement, the model was refitted to the OMIT electron-density map by the program *XtalView* (McRee, 1999). Water molecules were picked up from the difference maps on the basis of peak-height and distance criteria (Morris *et al.*, 2002). The same refinement procedure was applied to *Tt*HGPRTase–IMP and *Tt*HGPRTase–GMP but using the coordinates of the unliganded enzyme as the initial model. The quality of the models was validated with *PROCHECK* (Laskowski *et al.*, 1993). Refinement statistics are shown in Table 1. Structure diagrams were drawn using the program *PyMOL* (DeLano, 2002).

The atomic coordinates and structure factors for the unliganded enzyme, IMP complex and GMP complex have been deposited in the RCSB Protein Data Bank as entries 3acb, 3acd and 3acc, respectively.

3. Results and discussion

3.1. Enzymatic activity

From the HPLC and mass-spectrometric analyses, the TTHA0220 protein showed phosphoribosyltransferase activity towards hypoxanthine and guanine but not xanthine. Thus, it was confirmed that the TTHA0220 protein is an HGPRTase. The kinetic constants for hypoxanthine were $k_{\rm cat} = 9.1 \pm 0.8\ {\rm s}^{-1}$ and $K_{\rm M} = 3.9 \pm 1.5\ \mu M$ and those for guanine were $k_{\rm cat} = 18 \pm 1\ {\rm s}^{-1}$ and $K_{\rm M} = 7.4 \pm 1.7\ \mu M$ at pH 7.8 and 298 K. The values for PRPP were $k_{\rm cat} = 20 \pm 2\ {\rm s}^{-1}$ and $K_{\rm M} = 68 \pm 18\ \mu M$ determined in the presence of 100 μM guanine. These values are consistent with those for *T. gondii* HGPRTase (Héroux, White, Ross, Davis *et al.*, 1999). These values are also consistent with those for human HGPRTase, except for the $K_{\rm M}$ values for guanine and hypoxanthine (Xu & Grubmeyer, 1998); those for *Tt*HGPRTase are ten times higher than those for the human enzyme. Furthermore, these values are also similar to those for other 6-oxopurine PRTases such as *T. cruzi* hypoxanthine PRTase (Canyuk *et al.*, 2004) as well as *P. falciparum* and *T. foetus* hypoxanthine–guanine–xanthine PRTases (Subbayya & Balaram, 2002; Munagala *et al.*, 1998).

3.2. Overall structure

The overall and subunit structures of *Tt*HGPRTase–IMP are shown with secondary-structure assignment by the program *DSSP* (Kabsch & Sander, 1983) in Figs. 2(*a*) and 2(*b*), respectively. *Tt*HGPRTase consists of 181 amino-acid residues with a molecular mass of 20 173 Da based on the primary structure. The enzyme consists of a hood domain (N-terminus to Ile14 and Asp153 to C-terminus) and a core domain (Ser15–Glu152). The hood domain contains a two-stranded β-sheet (β-strands b6 and b7) and loop IV, which is characterized by three hydrogen-bonded turns (Kabsch & Sander, 1983; Fig. 2*b*). The core domain has an α/β structure similar to the Rossmann fold, in which a five-stranded parallel β-sheet (β-strands b2, b1, b3, b4 and b5) is covered by three α-helices (a1, a2 and a3) and a 3_{10}-helix (a4). Loop II between b2 and b3 is largely disordered as observed in the unliganded forms and 6-oxopurine monophosphate complexes from other species (Schumacher *et al.*, 1996; Somoza *et al.*, 1996; Héroux, White, Ross & Borhani, 1999; Shi, Li, Tyler, Furneaux, Grubmeyer *et al.*, 1999; Shi, Li, Tyler, Furneaux, Cahill *et al.*, 1999; Héroux *et al.*, 2000; Guddat *et al.*, 2002; Keough *et al.*, 2005).

There is one subunit in the asymmetric unit and the polypeptide chain is folded into a dimeric form with a crystallographic twofold axis. The accessible surface area (ASA) of the subunit interface was calculated to be 2876 Å^2, meaning that a surface area equivalent to 18.4% of one subunit is buried upon dimerization. The subunit interface is formed by residues from loop I, a2, b2, the C-terminal region of loop II and loop IV. Subunit–subunit interactions are predominantly hydrophobic, with two salt bridges and four neutral hydrogen bonds. Loop I, loop II and loop IV are not only involved in the formation of the subunit interface but also in the formation of the active site. Therefore, dimerization of the enzyme might be essential for enzyme function, although all of the active-site residues which directly interact with the substrates are from one subunit (Subbayya & Balaram, 2002; Canyuk *et al.*, 2004).

The corresponding C^α atoms of *Tt*HGPRTase–IMP and *Tt*HGPRTase–GMP superimpose with an r.m.s.d. of 0.15 Å, indicating that the overall folds of these complexes are quite similar to each other. The unliganded form and *Tt*HGPRTase–IMP superimpose less well, with an r.m.s.d. of 0.34 Å (Fig. 2*c*). Marked

displacements of C^{α} atoms are found for Asp106 (0.99 Å), Arg137 (0.72 Å), Tyr155 (1.13 Å), Pro178 (0.96 Å) and Glu179 (0.97 Å). The binding of IMP to the active site induces movement of the main-chain atoms of Ala154, Tyr155 and Val156 towards IMP, resulting in the formation of hydrogen bonds between the main-chain C═O and NH groups of Val156 and the N1—H and C6═O groups of the IMP purine ring and the stacking of the side-chain phenyl ring of Tyr155 on the purine ring (Figs. 2*c* and 2*d*; Chen *et al.*, 2005). This movement is accompanied by a shift of the main-chain atoms of the residues Pro178 and Glu179 which are adjacent to residues 154–156. Asp106 is considered to act as a catalytic base to abstract a proton from N7—H of the purine ring (Xu & Grubmeyer, 1998). The catalytic Asp106, which is hydrogen bonded to the active-site water molecule in the unliganded form, changes its direction towards the solvent side and makes a salt bridge with Arg137 in the *Tt*HGPRTase–IMP complex. This occurs in order to avoid an unusually short contact between the

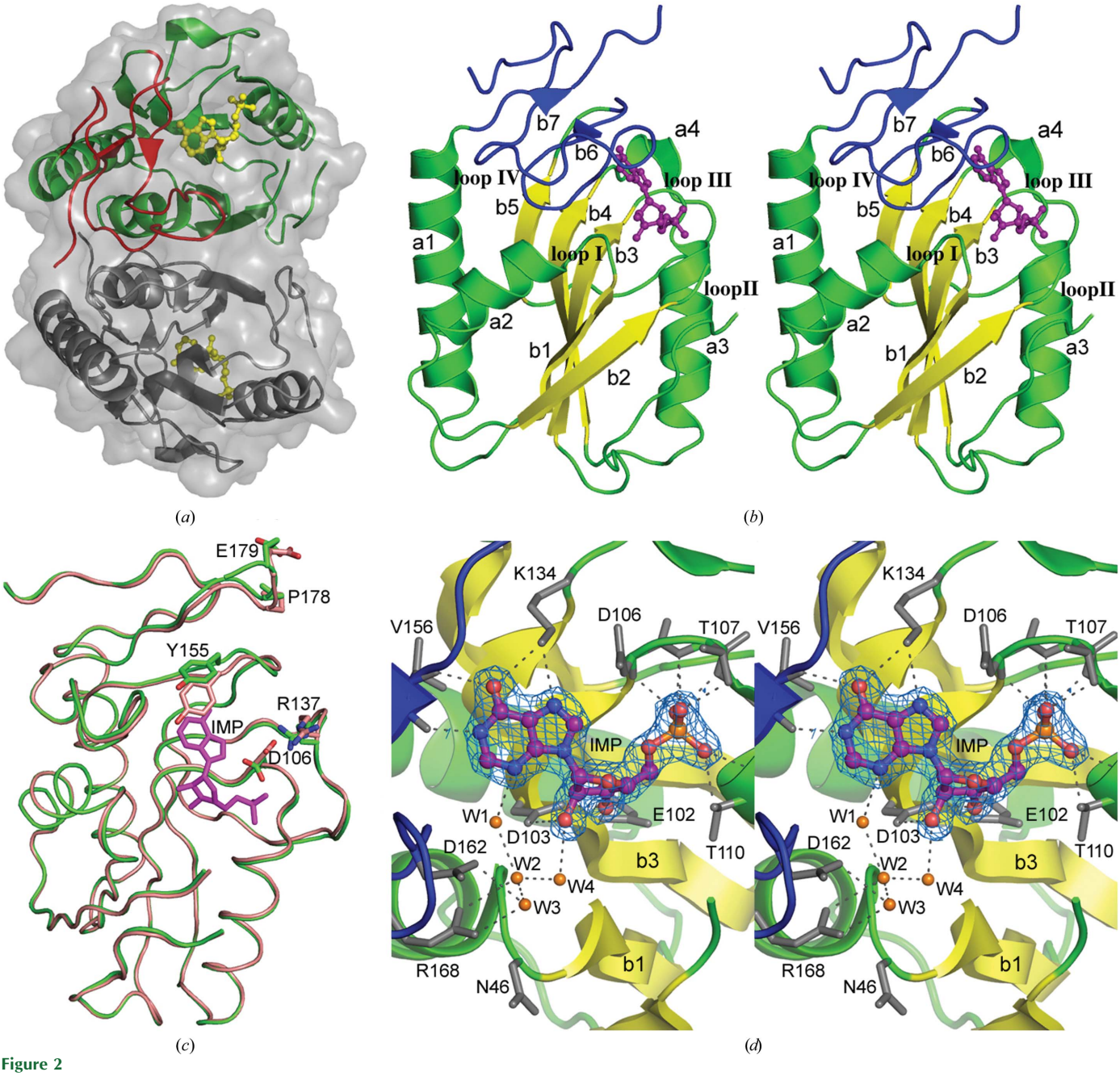

Figure 2
Overall and active-site structures of *Tt*HGPRTase–IMP. (*a*) View of the dimer perpendicular to the molecular twofold axis. IMP (yellow) is represented by a ball-and-stick model. The hood and core domains of one subunit are represented by secondary structures in red and green, respectively. The other subunit is shown in dark grey. (*b*) Stereoview of the subunit structure showing secondary-structure assignments. α-Helices (green) are denoted a1–a4 and β-strands (yellow) are denoted b1–b7. The hood domain is shown in deep blue. IMP (purple) is represented by ball-and-stick model. (*c*) Superimposition of the C^{α} atoms of unliganded *Tt*HGPRTase on those of *Tt*HGPRTase–IMP. The unliganded and complexed forms are drawn in green and salmon, respectively. IMP (pink) is represented as a stick model. The residues shown as stick models show significant movement on binding IMP. (*d*) Stereoview of the active site. IMP and active-site residues are represented by ball-and-stick and stick models, respectively. Hydrogen bonds are shown as dotted lines. Water molecules (W1–W4) shown by orange circles occupy the binding site of PRPP pyrophosphate. Tyr155, which stacks on the 6-oxopurine ring of IMP, is omitted for clarity. The OMIT electron-density map contoured at the 1.0σ level was calculated using data to 1.89 Å resolution.

carboxylate of Asp106 and the unprotonated N7 of the purine ring. It is reasonably assumed that the substrate hypoxanthine or guanine is bound to the active site with the protonated N7 involved in the hydrogen bond to Asp106. The change from the attractive interaction between N7 and Asp106 in the enzyme–substrate complex to the repulsive interaction in the enzyme–product complex may assist in product (IMP or GMP) release from the active site.

3.3. Active-site structure

The active-site structure is shown in Fig. 2(*d*). IMP resides in the pocket formed at the topological switch point between the C-terminal sides of β-strands b1 and b3. The active-site cavity is encircled by Asn46, Tyr73, Glu102, Asp103, Asp106, Thr107, Gly108, Thr110, Lys134, Tyr155, Val156, Asp162 and Arg168, the side chains of which interact with the substrates. Tyr73, which belongs to loop II, is disordered in the apo and IMP-bound forms. The purine, ribose and phosphate moieties of IMP occupy positions similar to the corresponding positions of 6-oxopurine analogues and PRPPs in enzyme–substrate complex models (Eads *et al.*, 1994; Somoza *et al.*, 1996; Focia, Craig & Eakin, 1998; Héroux *et al.*, 2000; Guddat *et al.*, 2002; Chen *et al.*, 2005). The hydrogen-bond interactions between the active-site residues and IMP thus mimic enzyme–substrate interactions. The main-chain C═O and NH of Val156 form hydrogen bonds to N1—H and C6═O of the IMP purine ring as described above. Lys134 interacts with C6═O and N7 of the purine ring. The side-chain carboxylates of Glu102 and Asp103 form hydrogen bonds to O3′ and O2′ of the ribose ring, respectively. Loop III specifically interacts with the phosphate group of IMP. The main chain C═O and NH groups of Asp106, Thr107 and Thr110 and the side-chain OH of Thr107 and Thr110 are hydrogen bonded to phosphate O atoms. Water molecules W1–W4 occupy the pyrophosphate-binding site for PRPP (Focia, Craig & Eakin, 1998; Balendiran *et al.*, 1999; Shi, Li, Tyler, Furneaux, Grubmeyer *et al.*, 1999; Shi, Li, Tyler, Furneaux, Cahill *et al.*, 1999; Héroux *et al.*, 2000; Canyuk *et al.*, 2001, 2004).

3.4. Structural comparison of 6-oxopurine PRTases

The program *SSM* (*Secondary Structure Matching*; Krissinel & Henrick, 2004) was used to search the Protein Data Bank for 6-oxopurine PRTase proteins that possess three-dimensional structures similar to that of *Tt*HGPRTase. The highest *Q*-scores were calculated to be 0.80 for *Salmonella typhimurium* 6-oxopurine PRTase (44% sequence identity; PDB code 1j7j; C. C. Lee, P. J. Focia, G. Spraggon & A. E. Eakin, unpublished work), 0.79 for that from *E. coli* (44% sequence identity; PDB code 1g9t; Guddat *et al.*, 2002), 0.78 for that from *T. foetus* (42% sequence identity; PDB code 1hgx; Somoza *et al.*, 1996), 0.76 for that from *T. tengcongensis* (50% sequence identity; PDB code 1yfz; Chen *et al.*, 2005), 0.72 for that from *L. tarentolae* (39% sequence identity; PDB code 1pzm; Monzani *et al.*, 2007), 0.70 for that from *T. cruzi* (43% sequence identity; PDB code 1tc1; Focia, Craig, Nieves-Alicea *et al.*, 1998), 0.54 for that from *H. sapiens* (36% sequence identity; PDB code 1bzy; Shi, Li, Tyler, Furneaux, Grubmeyer *et al.*, 1999) and 0.53 for that from *T. gondii* (30% sequence identity; PDB code 1qk4; Héroux, White, Ross & Borhani, 1999). The C^{α} atoms of *Tt*HGPRTase were superposed on the corresponding atoms of these enzymes with average and maximum r.m.s.d.s of 1.05 and 1.22 Å, respectively, indicating that the overall fold of *Tt*HGPRTase is similar to those of 6-oxopurine PRTases determined to date by X-ray methods (Fig. 3). Importantly, the active-site structures of 6-oxopurine PRTases have quite a similar structure, guaranteeing the phosphoribosyltransferase activity of these enzymes. The *SSM* result shows that these enzymes can be tentatively divided into groups I (the first six enzymes plus *Tt*HGPRTase; Fig. 3*a*) and II (last two enzymes; Fig. 3*b*) on the basis of *Q*-scores. The gap in *Q*-scores between groups I and II is at least

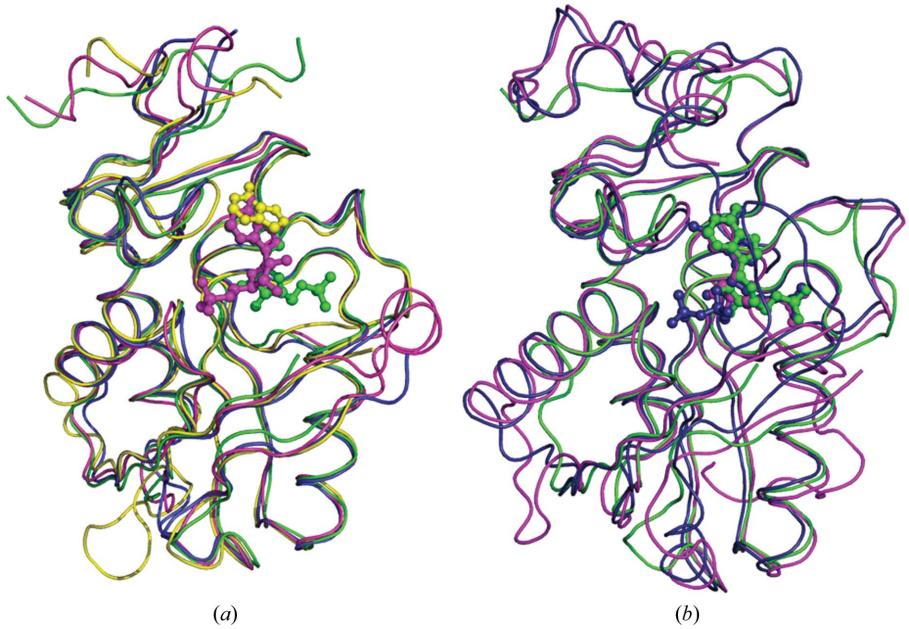

(*a*) (*b*)

Figure 3
(*a*) Superimposition of *Tt*HGPRTase–IMP (green) onto selected group I enzymes. The enzymes from *S. typhimurium* (PDB code 1j7j), *Ta. tengcongensis* (1yfz) and *Try. cruzi* (1tc1) are shown in deep blue, pink and yellow, respectively. The enzymes and their ligands are shown in the same colours. The ligands shown as ball-and-stick models are IMP (green), IMP (pink) and formycin B (yellow). The phosphate group of IMP bound to *Ta. tengcongensis* HGPRTase is located at a position that is quite different from that of IMP bound to *Tt*HGPRTase. (*b*) Superimposition of *Tt*HGPRTase–IMP (green) onto the group II enzymes. The enzymes from *H. sapiens* (PDB code 1bzy) and *Tox. gondii* (1qk4) are shown in deep blue and pink, respectively. The ligands are IMP (green), immucillin GP (deep blue; Shi, Li, Tyler, Furneaux, Grubmeyer *et al.*, 1999; Shi, Li, Tyler, Furneaux, Cahill *et al.*, 1999), pyrophosphate (deep blue) and IMP (pink).

partly a consequence of the fact that the group II enzymes have an N-terminal extension with additional secondary elements and a long loop connecting α-helix a2 and β-strand b2 compared with the group I enzymes.

*Tt*HGPRTase is folded into a functional dimer in the group I enzymes from *T. foetus*, *T. cruzi* and *L. tarentolae*. In contrast, in the group I enzymes from *S. typhimurium*, *E. coli* and *T. tengcongensis* and the group II enzymes from *H. sapiens* and *T. gondii* two functional dimers associate to form the tetramer. The tetramer interfaces of *H. sapiens* and *T. gondii* 6-oxopurine PRTases (the group II enzymes) are predominantly formed by the N-terminal extension and the subsequent α-helix a1. In *T. tengcongensis*, *S. typhimurium* and *E. coli* (the group I enzymes), loop II containing the region between β-strands b2 and b3 and α-helix a3 forms the tetramer interface. Tetramer interfaces are not involved in the formation of the active site in either the group I or II enzymes. These results imply that the dimers common to 6-oxopurine PRTases are essential for catalytic activity and the tetramer is considered to be a dimer of functional dimers.

Of the 13 active-site residues in *Tt*HGPRTase, Lys134, Asp106, Thr107, Thr110, Tyr73, Glu102, Asp103, Asp162 and Arg168 are completely conserved among the 6-oxopurine PRTase structures determined to date by X-ray methods, although Thr107 is replaced by Ser in some cases (Fig. 2*d*). The side chains of these residues are involved in interactions with the substrates. The remaining three residues (Gly108, Val156 and Asn46), the main chains of which are hydrogen bonded to the substrates, are Gly or Ala, Val or Ile and a hydrophilic or a positively charged residue, respectively. The overall folds and the active-site structures of 6-oxopurine PRTases are similar for both unliganded forms and product-complex models, although the binding of IMP or GMP induces a small conformational change and the binding of substrate analogues containing pyrophosphate further induces a movement of loop II to encapsulate the substrates from the solvent region (Somoza *et al.*, 1996; Focia, Craig, Nieves-Alicea *et al.*, 1998; Shi, Li, Tyler, Furneaux, Grubmeyer *et al.*, 1999; Héroux *et al.*, 2000; Guddat *et al.*, 2002; Canyuk *et al.*, 2004; Chen *et al.*, 2005). The *cis*-peptide bond in loop I, Leu45–Asn46, is a common feature of the phosphoribosyltransferare family (Canyuk *et al.*, 2004) and this conformation is also not affected by the ligand binding.

The ribose 5′-phosphate moiety of IMP is bound to *T. tengcongensis* HGPRTase in an unusual position that differs from the common binding site in other 6-oxopurine PRTase complexes with IMP (Chen *et al.*, 2005). The 2-OH and 3-OH groups of the ribose in *T. tengcongensis* HGPRTase are directed towards the solvent region and the 5-phosphate occupies the binding site for the pyrophosphate of PRPP (Fig. 3*a*). IMP trapped in the unusual position was modelled into the active site of *Tt*HGPRTase by superimposing *T. tengcongensis* HGPRTase onto *Tt*HGPRTase. The modelled IMP could be bound to *Tt*HGPRTase without any clashes with the protein residues surrounding the active site and its phosphate group interacted with the side chains of Arg168 (Arg167 in *T. tengcongensis* HGPRTase) and the main-chain NH groups of Gly47 (Gly46) and Asn46 (Lys45), just like IMP in *T. tengcongensis* HGPRTase. It is possible that two binding sites are available for product release and feedback inhibition as pointed out by Chen *et al.* (2005). In *T. tengcongensis* HGPRTase the common binding site for the IMP phosphate in 6-oxopurine PRTases is partially occupied by acetate derived from the buffer solution. This might be the reason why IMP in *T. tengcongensis* HGPRTase selects the unusual pyrophosphate-binding (or feedback) position from the two available sites.

In conclusion, although many crystal structures of HGPRTase as well as of related enzymes have been determined, a set of high-resolution structures of TtHGPRTase in the apo, IMP-bound and GMP-bound forms add novel information about the structure and function of the phosphoribosyltransferase. Further analysis of this enzyme family, including that of adenine phosphoribosyltransferase from *T. thermophilus*, is in progress.

We gratefully acknowledge Ms Miwa Ohmori and Dr Hitoshi Iino for their technical contributions.

References

Balendiran, G. K., Molina, J. A., Xu, Y., Torres-Martinez, J., Stevens, R., Focia, P. J., Eakin, A. E., Sacchettini, J. C. & Craig, S. P. III (1999). *Protein Sci.* **8**, 1023–1031.

Brünger, A. T., Adams, P. D., Clore, G. M., DeLano, W. L., Gros, P., Grosse-Kunstleve, R. W., Jiang, J.-S., Kuszewski, J., Nilges, M., Pannu, N. S., Read, R. J., Rice, L. M., Simonson, T. & Warren, G. L. (1998). *Acta Cryst.* D**54**, 905–921.

Canyuk, B., Focia, P. J. & Eakin, A. E. (2001). *Biochemistry*, **40**, 2754–2765.

Canyuk, B., Medrano, F. J., Wenck, M. A., Focia, P. J., Eakin, A. E. & Craig, S. P. III (2004). *J. Mol. Biol.* **335**, 905–921.

Chen, Q., Liang, Y., Su, X., Gu, X., Zheng, X. & Luo, M. (2005). *J. Mol. Biol.* **348**, 1199–1210.

DeLano, W. (2002). *PyMOL Molecular Viewer.* DeLano Scientific, San Carlos, California, USA.

Eads, J. C., Scapin, G., Xu, Y., Grubmeyer, C. & Sacchettini, J. C. (1994). *Cell*, **78**, 325–334.

Focia, P. J., Craig, S. P. III & Eakin, A. E. (1998). *Biochemistry*, **37**, 17120–17127.

Focia, P. J., Craig, S. P. III, Nieves-Alicea, R., Fletterick, R. J. & Eakin, A. E. (1998). *Biochemistry*, **37**, 15066–15075.

Guddat, L. W., Vos, S., Martin, J. L., Keough, D. T. & de Jersey, J. (2002). *Protein Sci.* **11**, 1626–1638.

Héroux, A., White, E. L., Ross, L. J. & Borhani, D. W. (1999). *Biochemistry*, **38**, 14485–14494.

Héroux, A., White, E. L., Ross, L. J., Davis, R. L. & Borhani, D. W. (1999). *Biochemistry*, **38**, 14495–14506.

Héroux, A., White, E. L., Ross, L. J., Kuzin, A. P. & Borhani, D. W. (2000). *Structure*, **8**, 1309–1318.

Kabsch, W. & Sander, C. (1983). *Biopolymers*, **22**, 2577–2637.

Keough, D. T., Brereton, I. M., de Jersey, J. & Guddat, L. W. (2005). *J. Mol. Biol.* **351**, 170–181.

Krissinel, E. & Henrick, K. (2004). *Acta Cryst.* D**60**, 2256–2268.

Laskowski, R. A., MacArthur, M. W., Moss, D. S. & Thornton, J. M. (1993). *J. Appl. Cryst.* **26**, 283–291.

Lesch, M. & Nyhan, W. L. (1964). *Am. J. Med.* **36**, 561–570.

McRee, D. E. (1999). *J. Struct. Biol.* **125**, 156–165.

Monzani, P. S., Trapani, S., Thiemann, O. H. & Oliva, G. (2007). *BMC Struct. Biol.* **7**, 59.

Morris, R. J., Perrakis, A. & Lamzin, V. S. (2002). *Acta Cryst.* D**58**, 968–975.

Munagala, N. R., Chin, M. S. & Wang, C. C. (1998). *Biochemistry*, **37**, 4045–4051.

Navaza, J. (1994). *Acta Cryst.* A**50**, 157–163.

Otwinowski, Z. & Minor, W. (1997). *Methods Enzymol.* **276**, 307–326.

Schumacher, M. A., Carter, D., Ross, D. S., Ullman, B. & Brennan, R. G. (1996). *Nature Struct. Biol.* **3**, 881–887.

Shi, W., Li, C. M., Tyler, P. C., Furneaux, R. H., Cahill, S. M., Girvin, M. E., Grubmeyer, C., Schramm, V. L. & Almo, S. C. (1999). *Biochemistry*, **38**,9872–9880.

Shi, W., Li, C. M., Tyler, P. C., Furneaux, R. H., Grubmeyer, C., Schramm, V. L. & Almo, S. C. (1999). *Nature Struct. Biol.* **6**, 588–593.

Somoza, J. R., Chin, M. S., Focia, P. J., Wang, C. C. & Fletterick, R. J. (1996). *Biochemistry*, **35**, 7032–7040.

Subbayya, I. N. & Balaram, H. (2002). *FEBS Lett.* **521**, 72–76.

Ueno, G., Hirose, R., Ida, K., Kumasaka, T. & Yamamoto, M. (2004). *J. Appl. Cryst.* **37**, 867–873.

Ueno, G., Kanda, H., Hirose, R., Ida, K., Kumasaka, T. & Yamamoto, M. (2006). *J. Struct. Funct. Genomics*, **7**, 15–22.

Ueno, G., Kanda, H., Kumasaka, T. & Yamamoto, M. (2005). *J. Synchrotron Rad.* **12**, 380–384.

Ullman, B. & Carter, D. (1995). *Infect. Agents Dis.* **4**, 29–40.

Wang, C. C. (1984). *J. Med. Chem.* **27**, 1–9.

Xu, Y. & Grubmeyer, C. (1998). *Biochemistry*, **37**, 4114–4124.